

## Polymer Films on Electrodes. 25. Effect of Polymer Resistance on the Electrochemistry of Poly(vinylferrocene): Scanning Electrochemical Microscopic, Chronoamperometric, and Cyclic Voltammetric Studies

Fu-Ren F. Fan, Michael V. Mirkin,<sup>†</sup> and Allen J. Bard\*

Department of Chemistry and Biochemistry, The University of Texas at Austin, Austin, Texas 78712

Received: September 23, 1993; In Final Form: November 30, 1993\*

The electrochemistry of a poly(vinylferrocene) (PVF) film of ca. 2100 Å was investigated in 1 M aqueous NaClO<sub>4</sub> solution with electrochemical and scanning microscopic techniques. The potential-step transients show well-defined maxima that are very similar to those found for the electrochemical switching of electronically conductive polymers, e.g., polypyrrole and polyaniline. We explore here the possibility that the film resistance accompanying changes in the polymer oxidation state is a major factor in determining the shape of these transients. These chronoamperometric curves also allow the determination of an apparent diffusion coefficient. The scanning electrochemical microscope (SECM) has been used to penetrate the PVF film and to obtain directly the thickness of the film immersed in the electrolyte solution. Different shapes of the tip current–distance curves are observed, depending on the oxidation state of the PVF film and its electrochemical treatment history. Mechanisms for the different approach curves are suggested.

### Introduction

Electrochemical oxidation and reduction of ionically and electronically conductive polymers has been extensively studied during the past decade.<sup>1</sup> Many publications have dealt with the mechanisms of charge and mass transport, heterogeneous and homogeneous electron transfer, counterion ejection and incorporation, and other phenomena contributing to polymer redox kinetics. However, further work is needed to build a self-consistent picture of these processes, particularly with respect to simulation of the voltammetric behavior. In a previous publication,<sup>2</sup> we demonstrated that scanning electrochemical microscopy (SECM) can provide valuable information about kinetic, charge transport, and thermodynamic parameters. Steady-state measurements with a conical nanometer-size ultramicroelectrode penetrating a thin polymer (Nafion) film loaded with an Os(bpy)<sub>3</sub><sup>3+/2+</sup> mediator were reported. The ionically conductive Nafion films are quite well behaved electrochemically; i.e., they are uniform, not very resistive, do not swell excessively, and demonstrate stable behavior relatively independently of the nature of the supporting electrolyte. In this publication, we apply the SECM technique in combination with chronoamperometry and cyclic voltammetry to study the oxidation/reduction behavior of a poly(vinylferrocene) film, whose electrochemistry is more complex.

One of the motivations for this study was a desire to explain the unusual shape of current–time curves for the oxidation of poly(vinylferrocene) (PVF) in aqueous solutions. The potential-step transients show well-defined maxima that are very similar to those found for the electrochemical switching of electronically conductive polymers, e.g., polypyrrole<sup>3</sup> and polyaniline.<sup>4</sup> The theory for the electrochemical behavior of electronically conductive polymers is complicated and incompletely understood (for different views, see, e.g., refs 5 and 6), and several explanations have been proposed for the unusual shape of transients. For example, these have been described in terms of the propagation of a metallike conductive phase,<sup>3b</sup> by nucleation-growth concepts,<sup>4</sup> or as “autocatalytic enhancement of the oxidation current”;<sup>6</sup> such models cannot be readily tested. In contrast, the electrochemistry of PVF is less complex.<sup>7,8</sup> An obvious parameter that depends on the polymer oxidation state is the effective resistance of the

polymer film, and we explore below the possibility that this resistance is a major factor in determining the shape of transients and voltammograms obtained at both macro- and microelectrodes. The effective resistance at a given point in a polymer film represents the combined effects of hindered electron transport to or from the point (e.g., by charge hopping between oxidized and reduced centers on the polymer chains) and the ionic transport of species from the solution phase (ionic migration) that compensate charge on the polymer produced by electron-transfer reactions. This effective resistance changes as a function of the degree of oxidation of a film, because of changes in the relative populations of oxidized and reduced sites as well as the ionic content of the film. It is also a factor in “first-cycle” or “breaking-in” effects.

The influence of the resistance on the behavior of modified electrodes was considered by many authors. For example, Roullier and Laviron<sup>9</sup> discussed cyclic voltammograms for a surface reaction with uncompensated *iR* drop. The resistance-caused deviations from Cottrell equation behavior<sup>10</sup> and the influence of solution resistance<sup>11</sup> were also considered, and a combination of resistive and capacitive effects was explored by means of digital simulation.<sup>12</sup> Recently, Buck and co-workers treated the resistive film problem analytically.<sup>13</sup> Unlike the previous reports, our model accounts for a change in polymer resistance in the oxidation/reduction process. The treatment closest to ours is that of Gottesfeld et al.<sup>14</sup> who simulated cyclic voltammograms assuming a changing film resistance. They, however, assumed the resistance to be a nonlinear function of the charge passed, which leads to an additional adjustable parameter that may not be necessary; they also assumed zero resistance for the polymer in one of its forms (reduced or oxidized). As shown below, this assumption is unsuitable for PVF.

### Model

The model described here is based on the usual finding that one oxidation state (reduced or oxidized) of a redox polymer, e.g., PVF, or an electronically conductive polymer, is significantly more resistive than the other. Thus, the oxidation or reduction of a polymer film should lead to a significant change in the effective ohmic resistance of a polymer-modified electrode. Consider a fixed site of thickness, *l*, on a metal substrate with a uniform

<sup>†</sup> Current address: Department of Chemistry, Queens College—CUNY, Flushing, NY 11367.

\* Abstract published in *Advance ACS Abstracts*, January 15, 1994.

distribution of redox centers of total concentration,  $c^*$ , where

$$c_{\text{Ox}} + c_{\text{Red}} = c^* = \text{const} \quad (1)$$

and the electronic conductivity is due to an electron exchange reaction (i.e., an electron-hopping mechanism). The hopping process can be described in terms of diffusion equations with a concentration dependent effective diffusion coefficient,  $D$ .<sup>15</sup> The diffusion problem for a thin layer of polymer initially containing only reduced electroactive moieties can be formulated as follows:

$$\frac{\partial c_{\text{Red}}}{\partial t} = D \frac{\partial^2 c_{\text{Red}}}{\partial z^2} \quad 0 < t, 0 < z \quad (2)$$

$$t = 0, 0 < z; \quad c_{\text{Red}}(t, z) = c^*; \quad c_{\text{Ox}}(t, z) = 0 \quad (3)$$

film/solution boundary:

$$0 < t, z = l; \quad \left. \frac{\partial c_{\text{Red}}(t, z)}{\partial z} \right|_{z=l} = 0 \quad (4)$$

metal/film boundary:

$$0 < t, z = 0; \quad \frac{i}{nFA} = D \left[ \frac{\partial c_{\text{Red}}(t, z)}{\partial z} \right]_{z=0} \quad (5)$$

where  $t$  is time,  $z$  is the coordinate in the direction normal to the electrode surface,  $l$  is the film thickness,  $A$  is the electrode surface area,  $i$  is the faradaic current,  $f = F/RT$ ,  $F$  is the Faraday, and  $c_{\text{Red}}$  and  $c_{\text{Red}}^s$  are the concentration of the reduced moiety and its surface ( $z = 0$ ) value, respectively.

We assume that the potential of the electrode with respect to the reference electrode is governed by the interfacial potential drop,  $E_1$ , and the resistive drop across the polymer film,  $E_2$ . We further assume that the electrode reaction is nernstian and the resistive potential drop in solution is negligible. Thus

$$E = E_1 + E_2 = E^{\circ'} + (RT/F) \ln [c_{\text{Ox}}^s/c_{\text{Red}}^s] - iR(t) \quad (6a)$$

$$E = E^{\circ'} + f^{-1} \ln [(c^* - c_{\text{Red}}^s)/c_{\text{Red}}^s] - iR(t) \quad (6b)$$

where  $E$  is the potential of the electrode,  $E^{\circ'}$  is the formal potential, and  $R(t)$  is the time-dependent resistance of the film. We take  $R(t)$  to be a linear function of the charge  $Q(t)$  passed during an oxidation/reduction process

$$Q(t) < Q_{\text{max}} \quad R(t) = R_1 + [Q(t)/Q_{\text{max}}](R_2 - R_1) \quad (7a)$$

$$Q(t) > Q_{\text{max}} \quad R(t) = R_2 \quad (7b)$$

$$Q(t) = \int_0^t i(\tau) d\tau \quad (7c)$$

where  $R_1$  and  $R_2$  are the film resistance values corresponding to the initial and final oxidation states, respectively, and  $Q_{\text{max}}$  is some limiting amount of charge after which further oxidation or reduction does not lead to any change in film resistance.  $Q_{\text{max}}$  is not necessarily the charge needed to completely oxidize (or reduce) the film during a potential step, because the resistance change could be associated with formation of ion-conductive channels in the polymer or solvent ejection and incorporation processes.

This model does not explicitly account for the effect of an electric field in the polymer, except for the ohmic resistance, nor for many other effects which can complicate significantly the behavior of conductive polymers.<sup>1,12,16</sup> We chose this simplified approach because it proved sufficiently accurate to provide a good quantitative fit between the theory and experimental results without the use of additional empirical parameters which can make the fit to experiment ambiguous and obscure conclusions

about reaction mechanisms. The solution of eqs 2–5 has been reported:<sup>17</sup>

$$c_{\text{Red}}^s(u) = c^* - \frac{l}{FDA} \int_0^u i(x) \theta_3(0|i\pi(u-x)) dx \quad (8)$$

where  $u = Dt/l^2$  and  $\theta_3$  is the theta function.<sup>18</sup> The combination of eqs 7 and 8 with the boundary conditions in eq 6 yields

$$1/\{1 + \exp[f(E - E^{\circ'} - i(u) R(u))]\} = 1 - \frac{l}{FDAc^*} \int_0^u i(x) \theta_3(0|i\pi(u-x)) dx \quad (9)$$

Equation 9 can be rewritten in terms of the dimensionless variable  $I(u) = i(u)l/(FDAc^*) = i(u)/i_d$ , where  $i_d$  is the steady-state diffusion limiting current (for a thin film,  $i_d = FDAc^*/l$ ), to yield

$$1/\{1 + \exp[f(E - E^{\circ'} - I(u) R(u) i_d)\} = 1 - \int_0^u I(x) \theta_3(0|i\pi(u-x)) dx \quad (10)$$

This equation was solved numerically (see Appendix). The solution of eq 10 for a given electrode potential depends on the parameters  $R_1 i_d$ ,  $R_2 i_d$ , and  $Q_{\text{max}}$ , which are adjusted to fit the experimental data.

Another experimental situation treated below involves an ultramicroelectrode (UME) positioned inside of a polymer film. Experimentally, the nanometer-sized UME is small compared to the film thickness, which can then be treated as infinitely thick. Assuming the UME to be a hemisphere of radius  $r$ , one can derive an integral equation analogous to eq 10:

$$1/\{1 + \exp[f(E - E^{\circ'} - J(y) R(y) i_d)\} = 1 - \int_0^y [1/\{\pi(y-x)^{1/2} - \exp(y-x) \text{erfc}((y-x)^{1/2})\}] J(x) dx \quad (11)$$

where  $y$  is the normalized time equal to  $Dt/r^2$  and  $J$  is the normalized faradaic current equal to  $i/i_d$  (where  $i_d$ , the steady-state diffusion limiting current for a hemisphere, is given by  $i_d = 2\pi FDr c^*$ ). The resistance with a hemispherical electrode of radius  $r$  in a uniform medium is  $R = \sigma/(2\pi r)$ ,<sup>19</sup> where  $\sigma$  is resistivity. When the UME, initially placed in a uniform medium with a resistivity  $\sigma_1$  oxidizes (or reduces) the polymer potentiostatically, the thickness of the newly formed zone (whose resistivity is  $\sigma_2$ ) should grow proportionally to  $t^{1/2}$ . Thus the resistance at the UME can be expressed as

$$R(t) = \sigma_2/(2\pi r) + (\sigma_1 - \sigma_2)/[2\pi(r + (Kt)^{1/2})] \quad (12)$$

where  $K$  is an arbitrary constant characterizing the propagation rate.

The theory for a steady-state process is much simpler. For a one-electron nernstian reduction at any uniformly accessible electrode, the steady-state current is

$$i = \frac{i_d}{1 + \exp[f(E - E^{\circ'} + Ri)]} \quad (13)$$

where  $i_d$  is the diffusion limiting current. From eq 13, one can deduce the resistance value from the steady-state current measured at a known potential

$$R = \left( E - E^{\circ'} + \frac{1}{f} \ln [(i_d - i)/i] \right) / i \quad (14)$$

or

$$Ri_d = \left( E - E^{\circ'} + \frac{1}{f} \ln [(1 - I)/I] \right) / I \quad (15)$$

Thus, the uncompensated resistive drop can be found at a given current from the deviation of the shape of the current-potential behavior (e.g., at an UME) from that expected for a nernstian process. A family of working curves,  $Ri_d$  vs  $I$ , calculated for different values of  $E - E^{\circ'}$  is shown in Figure 1.

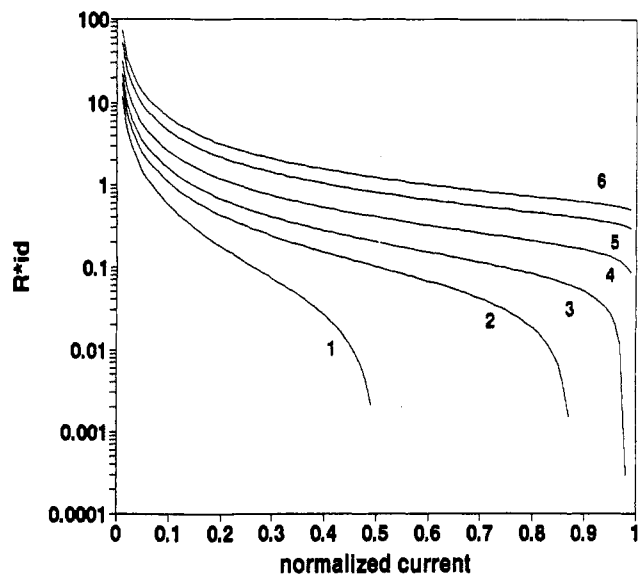


**Figure 1.** Working curves expressing the ohmic potential drop (as  $Ri_d$  in V) as a function of normalized current ( $i/i_d$ ) for different values of  $E^{o'} - E$  computed from eq 15: (1) 0, (2) 0.05, (3) 0.1, (4) 0.2, (5) 0.4, and (6) 0.6 V.

### Experimental Section

**Materials.** Poly(vinylferrocene) (PVF) was 15 700 molecular weight (degree of polymerization 74).<sup>7b</sup> Indium tin oxide (ITO) on glass (Delta Technologies, Inc., Stillwater, MN) was degreased in trichloroethylene (Aldrich, Milwaukee, WI) and was subsequently washed with ethanol and dried in air before use. Chlorobenzene (Fisher Scientific, Fair Lawn, NJ) was used as the solvent for PVF. All other chemicals were reagent grade and were used without further purification. Millipore reagent water was used for the preparation of aqueous solutions. Pt-Ir (80%–20%) rods (0.125- or 0.250-mm diameter) were obtained from FHC Co. (Brunswick, ME). All experiments were carried out in ambient.

**Preparation of Ultramicrotips and Substrate.** PVF coatings were applied to ITO substrates by spin coating a PVF solution in chlorobenzene (1% w/v) at a rotation speed of 3000 rpm with a photoresist spinner (Headway Research Inc., Garland, TX). The film was dried in air overnight before use.

The ultramicrotips used in this experiment were prepared based on the procedures described previously,<sup>20</sup> with some modifications. A 125- or 250- $\mu\text{m}$ -diameter Pt-Ir rod was sharpened by electrochemical etching in a solution consisting of saturated  $\text{CaCl}_2$  (60% by volume),  $\text{H}_2\text{O}$  (36%), and  $\text{HCl}$  (4%) at ca. 25 V rms ac applied with a Variac transformer. A carbon plate served as the counterelectrode in a two-electrode cell. After etching, the tip was washed with Millipore reagent water and ethanol and then dried in air prior to insulation. Insulation of the tip was done with Apiezon wax following the procedure reported by Nagahara et al.<sup>21</sup> Several coatings were usually required to insulate the tip completely or nearly completely. The insulated tip was then mounted on an electrochemical scanning tunneling microscope (STM) immersed in a solution containing a redox electrolyte (e.g., 20 mM  $\text{Fe}(\text{CN})_6^{4-}$  in 0.5 M  $\text{Na}_2\text{SO}_4$ ). The degree of insulation of the tip was checked by carrying out cyclic voltammetry. For a completely insulated tip, the very end of the tip was exposed in the STM by the following procedure. The potentials of the tip and a conductive substrate (e.g., a Pt or Au disk) were biased at suitable values (e.g., 0.80 V vs SCE for the tip and  $-0.20$  V for the substrate) with the STM in the constant current mode so that the tip approached the surface of the substrate. The onset of a current flow produced a hole in the tip insulation at the point of closest approach of tip to substrate, while leaving most of the tip still insulated. The amount of exposed

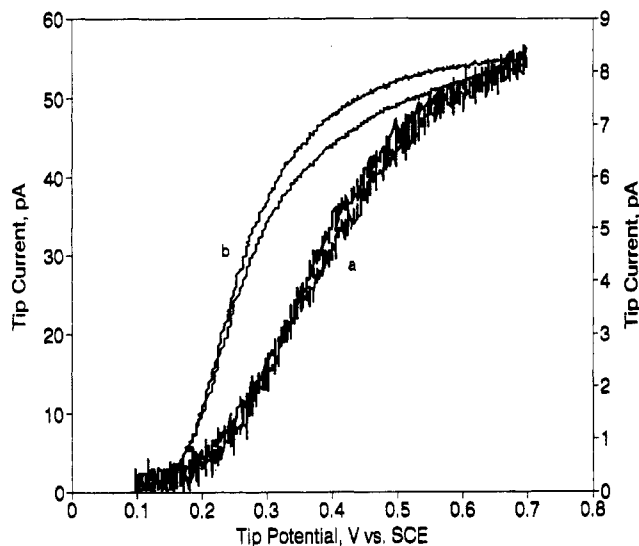


**Figure 2.** Cyclic voltammograms at an ultramicrotip electrode at an infinite distance from a Pt disk substrate (diameter = 5 mm) in a solution containing 20 mM  $\text{Fe}(\text{CN})_6^{4-}$  and 0.5 M  $\text{Na}_2\text{SO}_4$  as the supporting electrolyte. Scan rate, 10 mV/s. STM conditions for the tip preparation:  $E_T = 0.80$  V vs SCE,  $E_S = -0.20$  V vs SCE, the reference current for the STM feedback circuit = 50 pA, the approaching speed of the tip to the substrate surface = 800  $\text{\AA}/\text{s}$ , and the number of engagement and withdrawal steps = (a) one (current, right axis) and (b) three (current, left axis).

area of the tip could be controlled by the bias potentials on the tip (e.g.,  $E_T = 0.80$  V vs SCE) and the substrate (e.g.,  $E_S = -0.20$  V vs SCE), the reference current setting (e.g., 50 pA), the gain of the feedback circuit of the STM, the approach speed of the tip to the substrate surface (e.g., 800  $\text{\AA}/\text{s}$ ), and the number of engagement and withdrawal steps. The exposed area of the tip could be estimated in situ from the steady-state tip current with the tip far away from the substrate,  $i_{T,\infty}$ , by the equation for a disk-shaped UME:

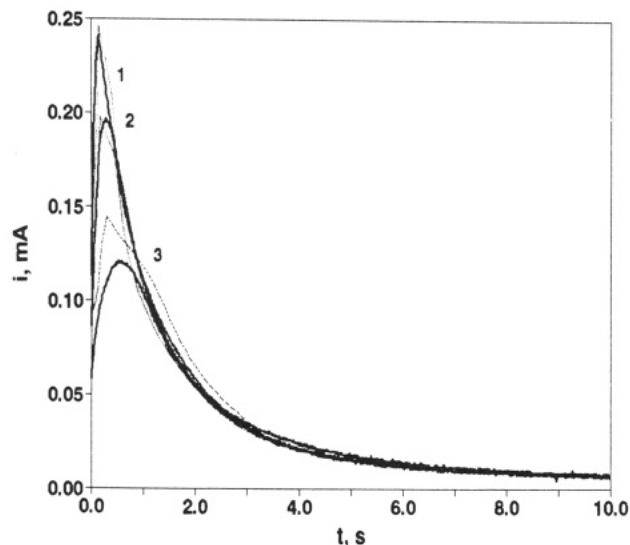
$$i_{T,\infty} = 4nFDcr \quad (16)$$

Figure 2 shows steady-state cyclic voltammograms (CVs) in 20 mM  $\text{Fe}(\text{CN})_6^{4-}$  and 0.5 M  $\text{Na}_2\text{SO}_4$  at a tip prepared by this technique. The equivalent tip radii,  $r$ , estimated from  $i_{T,\infty}$  were ca. 20  $\text{\AA}$  for a tip prepared after the first engagement and withdrawal step and ca. 140  $\text{\AA}$  for the same tip after the third engagement and withdrawal step.

**Apparatus.** STM, SECM, and electrochemical measurements were performed using an instrument described previously.<sup>22</sup> A custom-built bipotentiostat was used to apply potentials to the tip ( $E_T$ ) and substrate ( $E_S$ ). Two potential programmers, a PAR 175 universal programmer (Princeton Applied Research, Princeton, NJ) and an IBM EC 225 voltammetric analyzer, were employed to control  $E_T$  and  $E_S$  independently. Signals were controlled and data were collected and processed via a personal computer.

### Results and Discussion

**Polymer Electrode Potential-Step Transients.** Three current transients for PVF oxidation in 1 M aqueous  $\text{NaClO}_4$  solution (Figure 3) were obtained by stepping the potential of the metal substrate from 0 V (vs SCE) to different positive values, i.e., 0.8 V (curve 1), 0.7 V (curve 2), and 0.6 V (curve 3). The PVF films used in this experiment had previously been subjected to several oxidation/reduction cycles and then left in the reduced (PVF) state before the potential step shown. These potential values were 480, 380, and 280 mV more positive than the formal potential of PVF,  $E^{o'} = 0.32$  V vs SCE, found from cyclic voltammograms. The essential common feature of all of these transients is the presence of the current maximum rather than the monotonic



**Figure 3.** Experimental (thick solid curves) and calculated (thin curves) chronoamperograms of PVF oxidation in 1 M NaClO<sub>4</sub>. Potential step was from 0 V vs SCE to (1) 0.8 V, (2) 0.7 V, and (3) 0.6 V. Fitting parameters:  $R_1 = 3700 \Omega$ ,  $R_2 = 1930 \Omega$ ;  $i_d = F D A c^* / l = 7.64 \times 10^{-5}$  A,  $Q_{\max} = 26.5 \mu\text{C}$ .

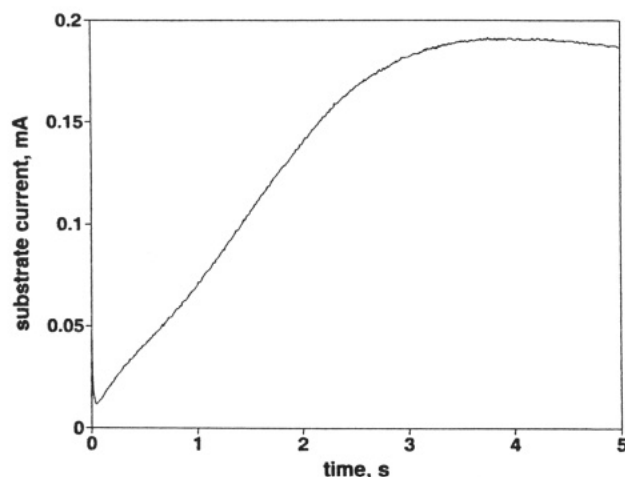


**Figure 4.** Experimental transient of the oxidation of the freshly prepared PVF film. Conditions were the same as for curve 1 in Figure 3.

(e.g.,  $t^{-1/2}$ ) decay usually observed in potential-step experiments. The peak current decreased and the corresponding time value increased with a decrease in potential (from curve 1 to curve 3). Theoretical curves shown in Figure 3 were calculated from eq 10, all with the same values of fitting parameters. Clearly, it was possible to fit curves 1 and 2 quantitatively, but for curve 3 the fit is not as good, probably because finite heterogeneous kinetics for electron transfer at the film/ITO interface become significant at the lower oxidation potential. The calculations demonstrate that a relatively small decrease in apparent ohmic resistance (by about a factor of 2) can result in the appearance of a sharp maximum on the chronoamperogram. The value of the charge passed,  $Q_{\max} = 26 \mu\text{C}$ , required for this change in resistance is significantly (about 10 times) lower than the total charge corresponding to complete oxidation of the film, perhaps for the reasons discussed above. The apparent diffusion coefficient value for all three curves was  $D = 2.1 \times 10^{-10} \text{ cm}^2/\text{s}$ , in good agreement with previously reported results.<sup>23</sup>

The chronoamperograms in Figure 3 were obtained after several oxidation/reduction potential cycles applied to the PVF film. In contrast, the transient presented in Figure 4 corresponds to the first oxidation (potential step from 0 to +0.8 V) of a freshly prepared PVF coating. The large changes in polymer morphology (breaking-in or first-cycle effect<sup>1</sup>) occurring along with the film

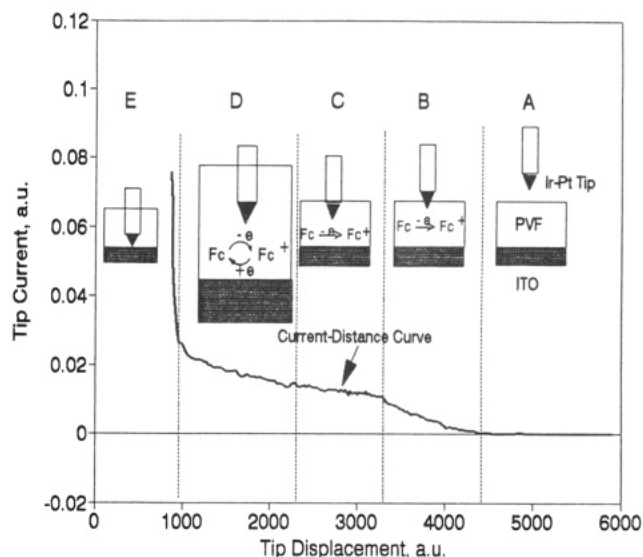


**Figure 5.** Schematic representation of the five stages of the SECM approach curve for a positively biased tip ( $E_T = 0.8 \text{ V}$ ) and a reduced PVF film ( $E_S = 0 \text{ V}$ ). (A) The tip is positioned in the solution close to the PVF/ITO. (B) The tip has penetrated partially into the PVF and the oxidation of PVF occurs. The effective tip surface grows with penetration. (C) The entire tip is in the PVF film but is still far away from the ITO surface. (D) The tip is sufficiently close to the ITO surface to observe positive SECM feedback. (E) The electron tunneling between tip and ITO occurs.

oxidation prevent one from quantitatively fitting the experimental data for this transient to the model. Our model in this case predicted qualitative features of the transient (an initial decrease in current and subsequent non-sharp maximum). It also indicated that the initial film resistivity in this case was about 8–10 times higher than that for a cycled film. This is in agreement with the picture of the freshly cast PVF film initially containing almost no water or supporting electrolyte and the presence of significant amounts of solvent and counterions in the film after cycling it in aqueous solution.<sup>24</sup>

**Scanning Electrochemical Microscope Experiments.** Information about PVF film characteristics was also obtained with the SECM. In this experiment, a small ( $\sim 25 \text{ nm}$ ) tip was moved into the film, which was immersed in electrolyte containing no electroactive species, through the film/solution interface into the film. An approach experiment of this type was discussed in detail earlier.<sup>2</sup> Figure 5 shows a scheme illustrating five stages of the SECM current–distance experiment and a representative approach curve: (A) Initially, the tip is in the solution near the PVF/electrolyte interface. Because the solution contains no electroactive species, a negligibly small current is observed before the tip touches the film surface. (B) When the tip starts to penetrate into the film, the tip current increases gradually until it reaches a limiting value. The increase represents the increasing area of the tip exposed to PVF film as the tip penetrates the polymer film. (C) When the tip is completely immersed in the film, but still a few tip diameters away from the ITO surface, the current levels off. (D) When the tip gets close to the substrate, the SECM positive feedback effect becomes important and the tip current increases. (E) Eventually, when the tip gets to within tunneling distance of the substrate, a very sharp increase in current occurs.

The tip current as a function of the relative tip displacement in the direction normal to the PVF/ITO substrate at several different values of tip and ITO bias is presented in Figure 6. Three pairs of approach curves are shown in Figure 6. Each pair of curves, a and d, b and e, and c and f, represents one set of data plotted on two different current scales, with curves a, b, and c corresponding to the less sensitive left-hand scale and curves d, e, and f corresponding to the finer right-hand scale. These three experiments represent substantially different situations: (1) the

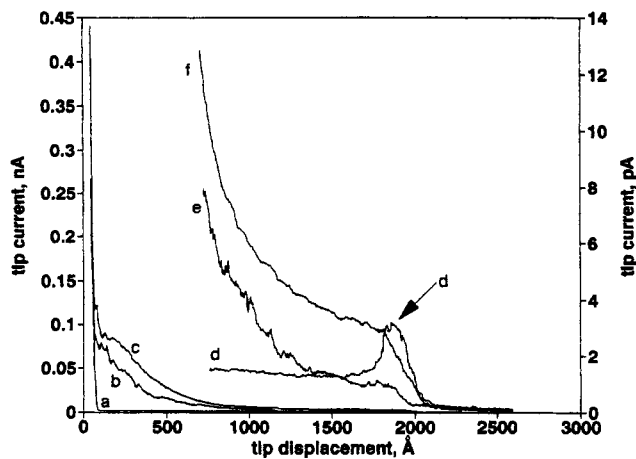


**Figure 6.** Dependencies of the tip current vs distance for a 25-nm-diameter Pt tip penetrating PVF films immersed in a 1 M NaClO<sub>4</sub> solution. The displacement values are given with respect to an arbitrary zero point. Curves a–c are at lower current sensitivity (left-hand scale). Curves d–f represent the same data at higher current sensitivity (right-hand scale); the tunneling current is too high to be shown on this scale. The tip moved at a rate of 30 Å/s. (a and d) The tip was biased at  $E_T = 0.8$  V vs SCE and the substrate at  $E_S = 0$  V vs SCE; PVF was freshly prepared. (b and e)  $E_T = 0.8$  V,  $E_S = 0.35$  V. (c and f)  $E_T = 0.8$  V,  $E_S = 0$  V; PVF was preoxidized at  $E_S = 0.8$  V vs SCE.

tip held at  $E_T = 0.80$  V vs SCE penetrates a preoxidized, reduced film ( $E_S = 0.00$  V) (curves c and f); (2) the tip at 0.80 V and PVF about half-oxidized ( $E_S = 0.35$  V, close to  $E^{\circ}$ ) (curves b and e); and (3) the tip at 0.80 V penetrates freshly prepared, reduced PVF ( $E_S = 0$  V) (curves a and d). From the low-sensitivity curves a–c, one can see that the tip current initially was small on this scale and increased sharply after the onset of tunneling when the tip approached the ITO substrate within the range of a few angstroms. Curves d–f offer a more detailed picture. Using the procedure described in ref 2, we found from curves e and f the height of the conical tip,  $h \approx 20$  nm, which is equal to the length of the interval between the onset of current and the plateau. This value is not very different from the tip radius,  $r = 14$  nm, found from the solution voltammetry. Thus the tip geometry can be roughly approximated with that of a 10–15 nm radius hemisphere.

In the first two cases (curves e and f), when the tip is completely immersed in the film but still far (i.e., greater than a few tip diameters) from the ITO substrate, the current remained constant and independent of tip position, as described in an analogous situation in ref 2. Without resistive effects, the expected plateau current on curve f would be about 2 times higher than on curve e, because the concentration of the reduced PVF moieties is about twice as high. More rigorous quantitative comparison is difficult, because the apparent diffusion coefficient can vary with potential.<sup>25</sup> When the tip moved deeper into the film, the current increases again due to the SECM positive feedback effect, and finally, when the tip gets to within tunneling distance of the substrate, a large increase in current occurs. The thickness of the film,  $l$ , can be found as a difference in relative displacement between the film/solution interface coordinate and that for the onset of tunneling, yielding  $l = 2100$  Å.

The current–distance curve d in Figure 6 differs substantially from the other two curves because the resistance of a freshly prepared reduced film is very high. In this case, the tip current, before leveling, reaches a maximum value and then decreases (Figure 7). This shape can be attributed to a change in film resistance near the tip electrode. This resistance should be roughly proportional to the thickness of the PVF layer between the tip and the electrolyte solution, i.e., to the distance measured from the point where the tip is completely immersed in the film (this corresponds to the maximum tip current). When the tip is deeply inside the PVF film, the resistance should be constant, independent of its position, and equal to  $\sigma/(2\pi r)$ . Curve 2 in Figure 7 is the

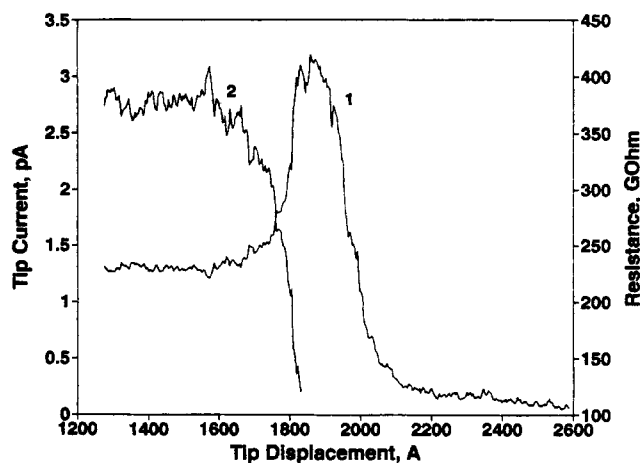


**Figure 7.** (Curve 1) detail of curve d from Figure 6 and (curve 2) corresponding resistance vs displacement dependence computed according to eq 15.

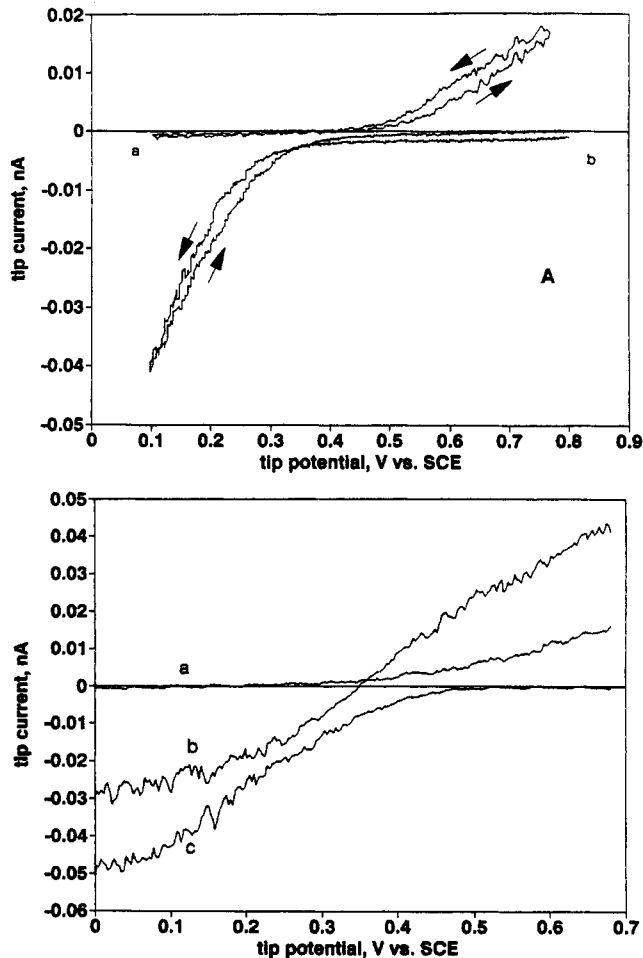


**Figure 8.** (A) Quasi-steady-state cyclic voltammograms of (a) oxidation and (b) reduction of PVF by a conical Pt tip partially penetrating the film. Substrate potential was (a) 0.1 V vs SCE and (b) 0.8 V vs SCE. (B) Voltammetric curves for the same process obtained at different substrate potentials: (a)  $-0.01$  V, (b) 0.35 V, and (c) 0.6 V. Potential sweep rate,  $\nu = 10$  mV/s.

dependence of resistance calculated by substitution of the current values from curve 1 into eq 15 upon tip displacement. The shape of curve 2 confirms the above qualitative prediction. At first the resistance grows linearly with the tip displacement and then levels off. A quite high effective resistivity,  $\sigma = 3 \times 10^6 \Omega \text{ cm}$ , was calculated from the limiting resistance value.

**Cyclic Voltammetry.** Figure 8A shows cyclic voltammograms of (a) oxidation and (b) reduction of PVF obtained at a tip UME

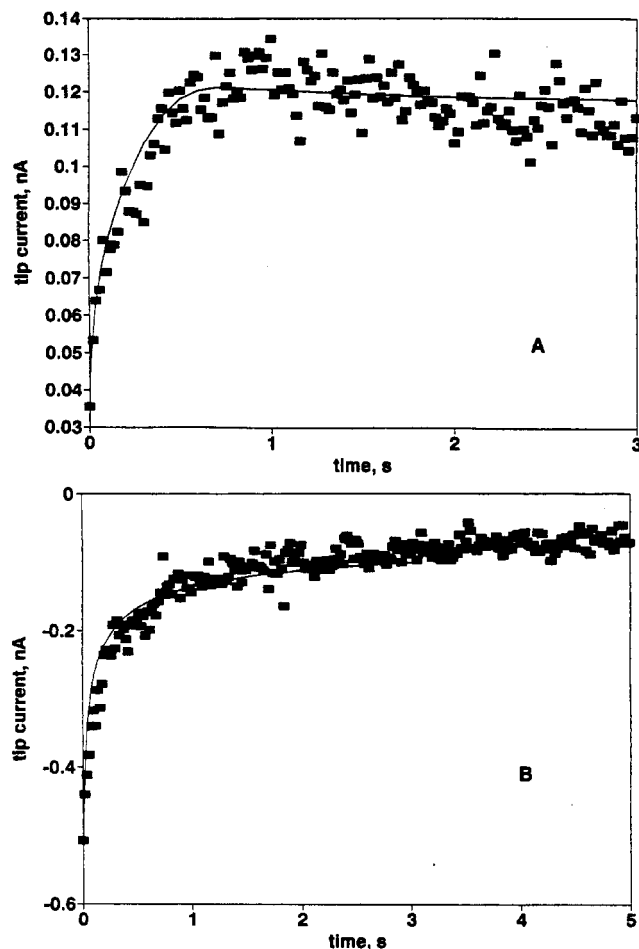


**Figure 9.** Chronoamperograms of PVF (A) oxidation and (B) reduction obtained at a nanometer-sized Pt tip inside the film. Potential step was (A) from 0 V vs SCE to 0.8 V and (B) from 0.6 to 0 V. Symbols are experimental data and solid curves are theory. Fitting parameters: (A)  $R_1 = 19 \text{ k}\Omega$ ,  $R_2 = 200 \text{ }\Omega$ ,  $i_d = 2\pi F D c^* r = 0.11 \text{ nA}$ ,  $K = 4 \times 10^{-11} \text{ cm}^2/\text{s}$ ; (B)  $R_1 = 600 \text{ }\Omega$ ,  $R_2 = 12.2 \text{ k}\Omega$ ,  $i_d = 3.2 \text{ nA}$ ,  $K = 2 \times 10^{-13} \text{ cm}^2/\text{s}$ .

partially inside the film (zone B in Figure 5) that display essentially ohmic behavior (i.e., a linear dependence of current on potential). The ratio between the slopes of the linear parts of these curves ( $di/dE$ ) allows one to compare effective resistivities of oxidized and reduced PVF. In agreement with the results extracted from Figure 3, the reduced PVF (curve a) appears to be about twice as resistive as its oxidized form. Analogously, a gradual decrease in effective resistance with the change of substrate potential in the positive direction can be deduced from the tip voltammetric curves shown in Figure 8b.

It has been suggested<sup>4</sup> that resistance effects in conductive polymer switching are primarily associated with  $iR$  drop in solution and could be diminished by using an UME instead of a conventional-sized substrate. If the change in polymer resistance is indeed the main factor determining the transient shape, the above model should be suitable for fitting data obtained with an UME of any size. Such results are presented in Figure 9. The potential of a nanometer-sized Pt tip electrode inside a PVF film was stepped (A) from 0 to 0.8 V vs SCE and (B) from 0.6 to 0 V. In the first case, the current transient corresponds to oxidation of PVF (substrate potential was 0.00 V vs SCE), and the film resistance decreased with time, leading to an increase in tip current. Conversely, the reductive transient of PVF (B) ( $E_s = 0.60 \text{ V vs SCE}$ ) led to an increase in  $R$ , and, thus, the tip current decreased monotonically. The film thickness (about 300 nm) was significantly larger than the UME radius, so the situation was treated in terms of eq 11. While a good fit between theory and experiment was obtained for both (A) oxidation and (B) reduction chronoamperograms, the values of parameters needed to fit these curves

were different. There are at least two reasons for this discrepancy: heterogeneous electron-transfer kinetics under nonsteady-state conditions at a small tip electrode were not rapid and the exact radius of the tip inside the film was unknown. Nevertheless, the resistivity values estimated from these chronoamperograms are of the same order of magnitude as those extracted from large substrate transients (Figure 3).

## Conclusions

This study has shown how the resistance change associated with the oxidation state of a PVF thin film affects its voltammetric and chronoamperometric behavior. It has also been shown how an ultramicrotip electrode in an SECM can penetrate a polymer film and be used to extract information about film thickness and the depth profile of film resistance. From the demonstrated increase in electrochemical activity of the PVF film during the first several oxidation/reduction cycles, we anticipate some microscopic structural change of the film, probably associated with ion and solvent permeation.

**Acknowledgment.** The support of this research by grants from the National Science Foundation (CHE9214480) and the Robert A. Welch Foundation is gratefully acknowledged.

## Appendix: Procedure for Numerical Solution of Eqs 10 and 11

Huber's method<sup>26</sup> was employed to solve eq 10 numerically. Previously,<sup>27</sup> a modified version of this method with a nonuniform temporal grid was used to accelerate significantly the solution of stiff kinetic equations. Since eq 10, describing a nernstian situation, is not stiff, the use of a uniform temporal grid is easier. The integral in eq 10 was calculated as

$$\int_0^u I(x)\theta_3(0|\pi(u-x)) dx = \sum_{i=1}^m a_i h_{m-i+1} \quad (\text{A1})$$

where  $a_i = [I(x_i) - I(x_{i-1})]\Delta x$ ,  $\Delta x = x_i - x_{i-1}$  is the integration step,

$$h_n = n\Delta x t_n - (n-1)\Delta x t_{n-1} + u_{n-1} - u_n \quad (\text{A2})$$

and

$$t_n = \int_0^{x_n} \theta_3(0|\pi x) dx; \quad u_n = \int_0^{x_n} x\theta_3(0|\pi x) dx \quad (\text{A3})$$

The substitution of eqs A1–A3 into eq 10 leads to a nonlinear algebraic equation. The  $i(u)$  value was found by numerical solution of this equation with the help of the subroutine ZBREN from the IMSL program library.<sup>28</sup>

The most time-consuming part of these calculations was the evaluation of the integrals in eq A3. We tried to use the approximations for these integrals suggested in ref 17b but found that eq 16' in that reference appears to be incorrect. Thus, the integrals in eq A3 were computed once using the subroutine QDAG<sup>28</sup> and were stored as an array for successive calculations. The numerical solution of eq 11 was completely analogous to the above.

## References and Notes

- (1) (a) Murray, R. W. In *Electroanalytical Chemistry*; Bard, A. J., Ed.; Marcel Dekker: New York, 1984; Vol. 13, p 191. (b) Hillman, A. R. In *Electrochemical Science and Technology of Polymers*; Lindford, R. G., Ed.; Elsevier, New York, 1987; p 103. (c) Inzelt, G. In *Electroanalytical Chemistry*; Bard, A. J., Ed.; Marcel Dekker: New York, 1994; Vol. 18, p 89.
- (2) Mirkin, M. V.; Fan, F.-R. F.; Bard, A. J. *Science* **1992**, *257*, 364.
- (3) (a) Pickup, P. G.; Osteryoung, R. A. *J. Electroanal. Chem.* **1985**, *195*, 271. (b) Aoki, K.; Tezuka, Y. *J. Electroanal. Chem.* **1989**, *267*, 55. (c) Abrantes, L. M.; Mesquita, J. C.; Kalaji, M.; Peter, L. M. *J. Electroanal. Chem.* **1991**, *307*, 275. (d) Mao, H.; Ochmanska, J.; Paulse, C. D.; Pickup, P. G. *Faraday Discuss. Chem. Soc.* **1989**, *88*, 165.

- (4) (a) Kalaji, M.; Peter, L. M.; Abrantes, L. M.; Mesquita, J. C. *J. Electroanal. Chem.* **1989**, *274*, 289. (b) Vuki, M.; Kalaji, M.; Nyholm, L.; Peter, L. M. *J. Electroanal. Chem.* **1992**, *332*, 315.
- (5) Feldberg, S. W. *J. Am. Chem. Soc.* **1984**, *106*, 4671.
- (6) Dolbhofer, K. *J. Electroanal. Chem.* **1992**, *331*, 1015.
- (7) (a) Merz, A.; Bard, A. J. *J. Am. Chem. Soc.* **1978**, *100*, 3222. (b) Peerce, P.; Bard, A. J. *J. Electroanal. Chem.* **1980**, *112*, 97; *114*, 89.
- (8) (a) Daum, P.; Lenhard, J. R.; Rolison, D. R.; Murray, R. W. *J. Am. Chem. Soc.* **1980**, *102*, 4649. (b) Daum, P.; Murray, R. W. *J. Phys. Chem.* **1981**, *85*, 389.
- (9) Roullier, L.; Laviron, E. *J. Electroanal. Chem.* **1983**, *157*, 193.
- (10) Richtering, W.; Dolbhofer, K. *Electrochim. Acta* **1989**, *34*, 1685.
- (11) Paulse, C. D.; Pickup, P. G. *J. Phys. Chem.* **1988**, *92*, 7002.
- (12) Yap, W. T.; Durst, R. A. *J. Electroanal. Chem.* **1987**, *216*, 11.
- (13) (a) Buck, R. P.; Nahir, T. M.; Mackel, R.; Liess, H.-D. *J. Electrochem. Soc.* **1992**, *139*, 1611. (b) Nahir, T. M.; Buck, R. P. *J. Electroanal. Chem.* **1992**, *341*, 41.
- (14) Gottesfeld, S.; Redondo, A.; Rubinstein, I.; Feldberg, S. W. *J. Electroanal. Chem.* **1989**, *265*, 15.
- (15) (a) Dahms, H. *J. Phys. Chem.* **1968**, *72*, 362. (b) Ruff, I.; Botar, L. *Chem. Phys. Lett.* **1986**, *126*, 348.
- (16) Anson, F. C.; Blauch, D. N.; Saveant, J. M.; Shu, C.-F. *J. Am. Chem. Soc.* **1991**, *113*, 1922, and references therein.
- (17) (a) Aoki, K.; Tokuda, K.; Matsuda, H. *J. Electroanal. Chem.* **1983**, *146*, 417. (b) Aoki, K.; Tokuda, K.; Matsuda, H. *J. Electroanal. Chem.* **1984**, *160*, 33.
- (18) Bateman, H. *Tables of Integral Transforms*; McGraw-Hill: New York, 1954; Vol. 1, p 388.
- (19) Newman, J. J. *Electrochem. Soc.* **1966**, *113*, 501.
- (20) Mirkin, M. V.; Fan, F.-R. F.; Bard, A. J. *J. Electroanal. Chem.* **1992**, *328*, 47.
- (21) Nagahara, L. A.; Thundat, T.; Lindsay, S. M. *Rev. Sci. Instrum.* **1989**, *60*, 3128.
- (22) Fan, F.-R. F.; Bard, A. J. *J. Electrochem. Soc.* **1989**, *136*, 3216.
- (23) Inzelt, G.; Szabo, L. *Electrochim. Acta* **1986**, *31*, 1381.
- (24) (a) Hillman, A. R.; Loveday, D. C.; Bruckenstein, S. *J. Electroanal. Chem.* **1989**, *274*, 157. (b) Inzelt, G.; Bacskai, J. *Electrochim. Acta* **1992**, *37*, 647.
- (25) (a) Chidsey, C. E. D.; Murray, R. W. *J. Phys. Chem.* **1986**, *90*, 1479. (b) Hunter, T. B.; Tyler, P. S.; Smyrl, W. H.; White, H. S. *J. Electrochem. Soc.* **1987**, *134*, 2198.
- (26) Nicholson, R. S.; Olmstead, M. L. In *Electrochemistry: Calculations, Simulations, and Instrumentation*; Mattson, J. S., Mark, H. B., MacDonald, H. C., Eds.; Marcel Dekker: New York, 1972; p 119.
- (27) Mirkin, M. V.; Nilov, A. P. *Comput. Chem.* **1991**, *15*, 55.
- (28) IMSL MATH/LIBRARY.FORTRAN Subroutines for Mathematical Applications, Version 1.1, IMSL Inc., Houston, 1989.